PRAMANA
— journal of
physics

Vol. 74, No. 6
June 2010
pp. 945–959

Characteristics of the aluminum alloy plasma produced by a 1064 nm Nd:YAG laser with different irradiances

W F LUO[1,*], X X ZHAO[2], Q B SUN[1], C X GAO[1], J TANG[1], H J WANG[1] and W ZHAO[1]

[1]State Key Laboratory of Transient Optics and Photonics, Xi'an Institute of Optics and Precision Mechanics, Chinese Academy of Sciences, Xi'an 710119, China

[2]Physics Department, Xi'an University of Arts and Science, Xi'an 710065, China

[*]Corresponding author. E-mail: luowf@opt.ac.cn

MS received 26 November 2009; revised 22 January 2010; accepted 4 February 2010

Abstract. The plasma generated by 1064 nm Nd:YAG laser irradiation of aluminum alloy in air at atmospheric pressure was studied spectroscopically. The electron density inferred by measuring the Stark-broadened line profile of Si(I) 288.16 nm decreases with increasing distance from the target surface. The electron temperature was determined using the Boltzmann plot method with nine strong neutral aluminum lines. Due to the thermal conduction towards the solid target and radiative cooling of the plasma as well as conversion of thermal energy into kinetic energy, the electron temperature decreases both at the plasma edge and close to the target surface. Electron density and electron temperature were also studied as functions of laser power density. At the same time, the validity of the assumption of local thermodynamic equilibrium and the effect of self-absorption were discussed in light of the results obtained.

Keywords. Atomic emission spectroscopy; laser-induced breakdown spectroscopy; plasma.

PACS Nos 32.30.-r; 32.70.-n; 52.25.-b

1. Introduction

As a powerful spectrochemical analysis technique, laser-induced breakdown spectroscopy (LIBS) has gained a great amount of interest in recent years. With LIBS, a pulsed laser is focussed to vaporize and ionize a sample of material and when the laser irradiance exceeds the breakdown threshold of the material, a luminous plasma is created. By collecting the generated atomic emission from the laser-induced plasma, the elemental composition of the sample can be determined qualitatively and quantitatively [1–4].

This relatively new technique offers many well-known advantages over conventional spectroscopic techniques such as the electrode spark, the inductively coupled

plasma and the mass spectrometry [5]. LIBS provides real time, multi-element analysis. Atomization and excitation are completed in a single sampling. The plasma can be generated in liquid, gas, and both conducting and non-conducting solids. At the same time, LIBS is considered a non-destructive technique because only a submicrogram amount of material is required for analysis. It requires little or no sample preparation, and so real-time and *in-situ* analyses are possible [6]. All these features result in wide applicability of LIBS in different fields, such as monitoring traces in materials [7], detection of metals in the environment [8], production control in the steel industry [9], the analysis of wood preservers [10], the identification of pigments in paintings [11], the identification of alloys [12] and even in space exploration [13].

Besides the large number of scientific and practical applications of LIBS, the study of its basic mechanisms is still a great challenge, since laser ablation is a complicated process that is governed by many variables, and there is no universal model to completely describe this phenomenon. The plasma and its characteristics (electron density, temperature, spatial and temporal behaviour) depend on the target's thermophysical properties and laser beam parameters, such as laser pulse temporal duration and shape, laser wavelength and energy [14,15]. Moreover, chemical, physical and mechanical properties of the sample as well as the composition and pressure of the sample environment also influence the ablation process [16,17]. Shaikh *et al* [18–21] reported the measurement of the zinc, cadmium, mercury, aluminum plasma parameters produced by the fundamental, second, and third harmonics of the Nd:YAG laser. They found that the emission intensity of the spectral lines was stronger in the UV laser because of the higher ablation as compared to the visible and IR lasers. At the same time, they also found the effect of the ambient atmosphere (Ar, Ne and He) on the plasma parameters and the emission intensities were found to be maximum in the case of Ar environment than the Ne and He environment. Elhassan *et al* [22] studied the influence of pulse duration (nanosecond and femtosecond) at a wavelength of 248 nm on the laser-induced plasma parameters and the quantitative analysis results for elements such as Sn, Zn and Pb in different types of bronze alloys adopting LIBS in ambient atmosphere. In case of fs-laser pulses, the plasma emission is found to vary much more rapidly with time than in the case of ns-laser-produced plasma. A number of researches show that even the same experimental parameters will produce different effect on different elements. For example, Cristoforetti *et al* [23] observed that the emission intensity of the Cu(I) line at 521.5 nm increases with the background gas pressure up to approximately 100 Torr and then it slightly decreases up to the atmospheric pressure. However, a different behaviour of the O(I) line at 777.3 nm was reported. All of these demonstrate that the mechanisms governing the laser–material interaction are complex and many cannot yet be accurately predicted and require further research. Furthermore, from the viewpoint of field-based and industrial applications, performing experiments in air at atmospheric pressure is more practical to help improve the capability and the ease of the on-line sample analysis.

The main motivation of the present study is to investigate the emission characteristics of laser-induced aluminum alloy plasma in air at atmospheric pressure in terms of spectral intensity, electron density and excitation temperature. The experiment was carried out using a Q-switched Nd:YAG (1064 nm) laser.

Emphases are given on their dependence on the laser power density and their spatial evolution. On the one hand, studying the spatial distribution of metal plasma produced by laser ablation can help to further understand the laser–matter interaction mechanism. On the other hand, the practical application of this technique also is beneficial, e.g. material processing, thin film deposition. Excitation temperature is estimated using the Boltzmann plot method with nine neutral Al transition lines, while the electron number density is determined from the Stark broadening of the neutral 288.158 nm silicon emission line. We found the electron temperature to be decreasing at both the plasma edge and close to the target surface, which is different from other findings in the literature [18–21]. Three possible reasons are put forward to explain this phenomenon. The relative transition probability ratio of two neutral Al lines at 308.215 and 309.284 nm has been determined using their relative line intensity ratio. The average values of the experimentally obtained transition probability ratios are in excellent agreement with the NIST database within the uncertainty, and their variations with different laser power densities are also studied. In addition, the local thermodynamic equilibrium (LTE) assumption and self-absorption are also discussed with the experimental results.

2. Experimental set-up

The experimental arrangement used is schematically depicted in figure 1. The laser source employed is a Q-switched Nd:YAG laser (1064 nm, 19.7 ns FWHM, 1 Hz, SGR, Beamtech Optronics). The pulse energy varying from about 20 mJ to 140 mJ was adjusted by changing the pumping power and controlled by a calibrated energy meter bought from National Institute of Metrology, China. The maximum shot-to-shot energy fluctuation was 6% which was the principal source of uncertainty in our measurements. The laser beam was focussed with a 150 mm focal length

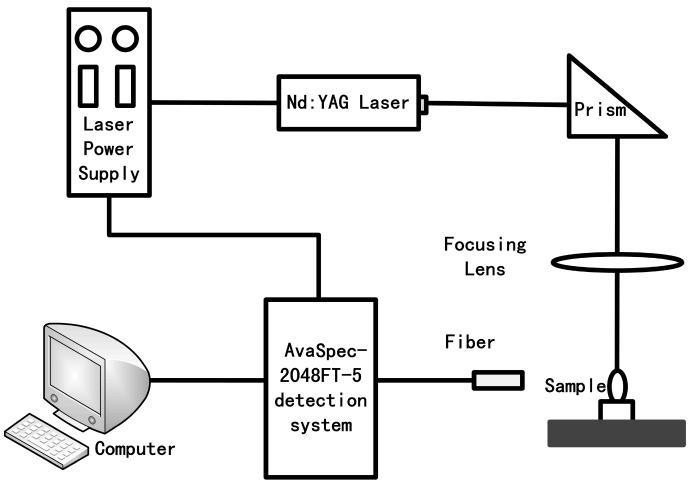

Figure 1. Experimental arrangement.

Table 1. Composition of the E414d aluminum alloy sample (wt%).

Si	Fe	Cu	Mn	Mg	Ni	Zn	Ti	Ga	Al
0.341	0.345	0.039	0.026	0.020	0.059	0.052	0.022	0.029	Remainder

quartz lens. The lens-to-sample distance was chosen to be slightly shorter than the focal length of the focussing lens in order to reduce the breakdown of the ambient gas in front of the target and ensure that most of the energy was deposited into the bulk material of the sample. The beam radius after focussing was 100 ± 10 μm measured with a microscope (OLYMPUS BX51). For the present study, seven different incident power densities of 3.7, 6.3, 9.7, 12.4, 15.9 19.0 and 21.9 GW/cm^2 were used. The sample was on top of an XYZ translation stage which was used for changing the focussing point so that the plasma was formed in each measurement on the smooth surface of the target.

The light emitted from the plasma was collected via AvaSpec-2048FT-5 detection system (Avantes, Holland) in conjunction with an optical fibre (200 μm in diameter) placed orthogonal to the direction of the plasma expansion with a minimum integrated time of 2 ms and a delay time of 5 μs. The emission signal was corrected by subtracting the dark signal of the detector through the software of the detection system. The AvaSpec-2048FT-5 detection system, covering the range between 200 nm and 720 nm and calibrated by the manufacturer using the standard light source, is equipped with five spectrometers. Each spectrometer has a slit width of 10 μm and 2048 element linear CCD array with an optical resolution of about 0.06 nm and 2400 grooves/mm. The AvaSpec-2048FT-5 detection system was triggered by the Q-switch of the Nd:YAG laser. The output data were averaged with six laser shots and stored in a personal computer through AvaSoft-LIBS for subsequent analysis.

The sample analysed was a certified aluminum alloy (reference E414d, Shanghai Research Institute of Materials, China) with traces of silicon, manganese and other metals. Its composition is given in table 1. Its surface was manually polished with sandpaper and washed with acetone each time. All the experiments were performed at room temperature in air at atmospheric pressure.

3. Results and discussion

3.1 *Plasma emission and spectral line analysis*

Figure 2 shows the typical plot of a spectrum of the aluminum alloy plasma at a distance of 0.5 mm from the target surface with an irradiance of 21.9 GW/cm^2. The laser-induced plasma spectrum consists of an intense continuum and a number of neutral as well as ionic lines of the component species. At early plasma times, the signal is mostly dominated by the continuum emission which is attributed to the collision of electrons with ions and atoms and the recombination of electrons with ions. As time progresses, continuum background diminishes while ionic and atomic emission lines become dominant [2]. To obtain the best signal-to-background ratio (SBR), the delay time (5 μs), which is the time between the laser shot and the

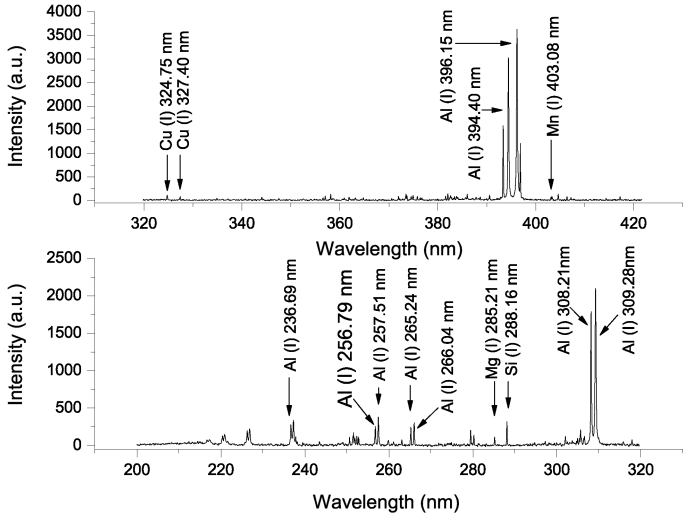

Figure 2. The typical emission spectrum generated by the 1064 nm laser at a distance of 0.5 mm from the target surface with an irradiance of 21.9 GW/cm^2.

initiation of data acquisition, is chosen in our experiments. The assignment of these atomic and ionic lines shown by the arrows in figure 2 was done using NIST database [24]. In our experiments, nine strong neutral aluminum lines at 236.69, 256.80, 257.51, 265.24, 266.04, 308.215, 309.284, 394.401 and 396.152 nm were used to determine the plasma temperature, while the Si(I) 288.158 nm emission line was used to calculate the electron number density in the plasma for this line shows less interference with other emission lines. The relevant transition parameters for the Boltzmann method and for the calculation of the electron density are found in [21,24,25].

3.2 *Diagnostic method of the excitation temperature* T_e

The characterization of laser-induced plasmas by determining the parameters, such as the temperature, the electron density and the number densities of different species, is interesting because it provides a better understanding of these complex and versatile spectroscopic sources. Furthermore, plasma descriptions start by trying to characterize the properties of the assembly of atoms, molecules, electrons and ions rather than the individual species. If thermodynamic equilibrium exists, then plasma properties, such as the relative populations of energy level and the distribution of the speed of the particles, can be described through the concept of temperature [2]. Under the LTE condition, the kinetic temperature and the excitation temperature are identical and can be determined from the Boltzmann diagram method. The population of the excited states follows the Boltzmann distribution and their relative spectral line intensity I_{mn} is given as [3]

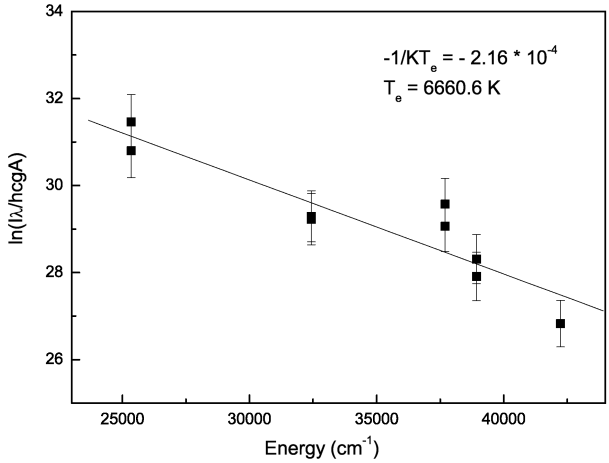

Figure 3. Boltzmann plot for temperature determination of a 1064 nm laser-induced plasma at a distance of 0.5 mm above the target surface with a laser power density of 6.3 GW/cm^2.

$$\ln\left(\frac{\lambda_{mn} I_{mn}}{h c g_m A_{mn}}\right) = -\frac{E_m}{k T_\mathrm{e}} + \ln\left(\frac{N(T)}{U(T)}\right), \tag{1}$$

where λ_{mn} is the wavelength, A_{mn} is the transition probability, g_m is the statistical weight of the upper level, h is the Plank constant and c is the speed of light in vacuum, E_m is the upper level energy, T_e is the electron temperature, k is the Boltzmann constant, $U(T)$ is the partition function and $N(T)$ is the total number density of species. Plotting the expression on the left-hand side of the equation vs. E_m yields a slope of $-1/(kT_\mathrm{e})$. The plasma temperature can be obtained even without knowing $N(T)$ or $U(T)$.

Figure 3 is a typical Boltzmann plot for temperature determination of the laser-induced plasma obtained at a distance of 0.5 mm from the target surface with a laser power density of 6.3 GW/cm^2, where the linear fit of the data is also shown. From the slope of -2.16×10^{-4}, the plasma temperature $T_\mathrm{e} = 6660.6 \pm 91.7$ K.

3.3 *Diagnostic method of the electron density* N_e

Electron number density is an important parameter that is used to describe a plasma environment and is also crucial for establishing thermodynamic equilibrium. One of the most powerful spectroscopic techniques to determine the electron number density with reasonable accuracy is the measurements of the Stark-broadened line profile of an isolated atom or singly charged ion [26]. For the estimation of electron number density, the Stark-broadened line profile of the 288.16 nm Si(I) emission line was used. In the experimental conditions of the present work, three broadening mechanisms are likely to contribute significantly to the linewidth observed in plasmas produced during pulsed laser ablation, viz. Doppler broadening, resonance pressure broadening and Stark broadening. The Doppler width due to

the random thermal motion of the emitter depends only on the absolute temperature and the atomic mass of the emitting species and is estimated using the relation [27]

$$\Delta\lambda_{\mathrm{D}} = 7.16 \times 10^{-7}\lambda\left(\frac{T_{\mathrm{e}}}{M}\right), \tag{2}$$

where $T_{\mathrm{e}}(K)$ is the electron temperature and M is the atomic mass. The Doppler effect causes a broadening of 0.0027 nm for Si(I) at 288.16 nm with $T_{\mathrm{e}} = 10000$ K much less than the minimum observed FWHM in our experiments. As the 288.16 nm Si(I) line is not associated with a resonance state, resonance broadening is negligible too. The Stark line broadening from the collision of the charged species is the primary mechanism influencing these emission spectra. The FWHM of the Stark-broadened line $\Delta\lambda_{1/2}$ is related to the electron density by the expression [25]

$$\Delta\lambda_{1/2} = 2w\left(\frac{N_{\mathrm{e}}}{10^{16}}\right) + 3.5A\left(\frac{N_{\mathrm{e}}}{10^{16}}\right)^{1/4} \times [1 - 1.2N_{\mathrm{D}}^{-1/3}] \times w\left(\frac{N_{\mathrm{e}}}{10^{16}}\right), \tag{3}$$

where $\Delta\lambda_{1/2}$ (nm) is the FWHM broadening of the line, w (nm) is the electron impact (EI) width parameter, A (nm) is the ion broadening parameter and N_{D} (cm^{-3}) is the number of particles in the Debye sphere [18].

The first term on the right side of eq. (3) represents the broadening due to electron contribution and the second term is the ion correction factor. The electric field that causes Stark effect in laser-induced plasmas results primarily from collisions with electrons, with small contributions due to collisions with ions [2]. Therefore, the FWHM broadening line $\Delta\lambda_{1/2}$ (nm) can be simplified to eq. (4)

$$\Delta\lambda_{1/2} = 2w\left(\frac{N_{\mathrm{e}}}{10^{16}}\right). \tag{4}$$

Typical Stark-broadened line profile is approximately Lorentzian and the experimental result at 0.5 mm above the target surface with an irradiance of 6.3 $\mathrm{GW/cm}^2$ is shown in figure 4 which fits fairly well with a typical Lorentzian profile.

3.4 *Effect of the laser irradiance on the plasma spectra, T_{e} and N_{e}*

Since LIBS is based on the spectral analysis of atomic emission from laser-induced plasma, the nature and characteristics of the laser-induced plasma strongly depend on the laser power density. To study the effect of the laser irradiance on the plasma parameters, the aluminum alloy was irradiated with different laser power densities (3.7, 6.3, 9.7, 12.4, 15.9, 19, 21.9 $\mathrm{GW/cm}^2$) and the detector was placed at a distance of 0.5 mm from the target surface. Figure 5 shows the variation of the plasma spectra with respect to the laser irradiance. For clarity, the variations of four neutral emission lines at 308.24, 309.28, 394.40 and 396.15 nm with the laser power density were specifically plotted in figure 6. As a whole, it is observed that

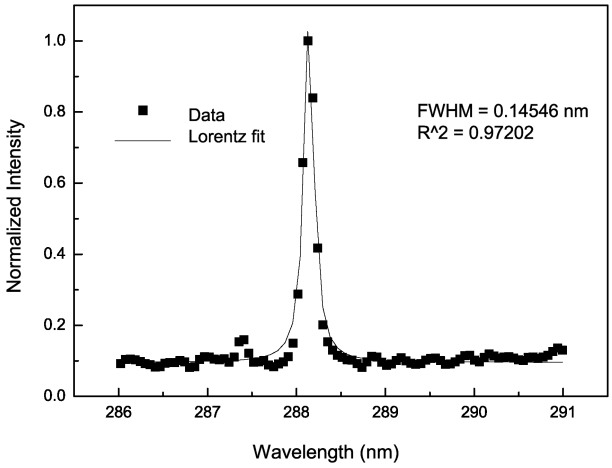

Figure 4. Typical Stark-broadened profile of Si(I) at 288.16 nm for 1064 nm irradiation at a distance of 0.5 mm from the target surface with a laser power density of 6.3 GW/cm^2.

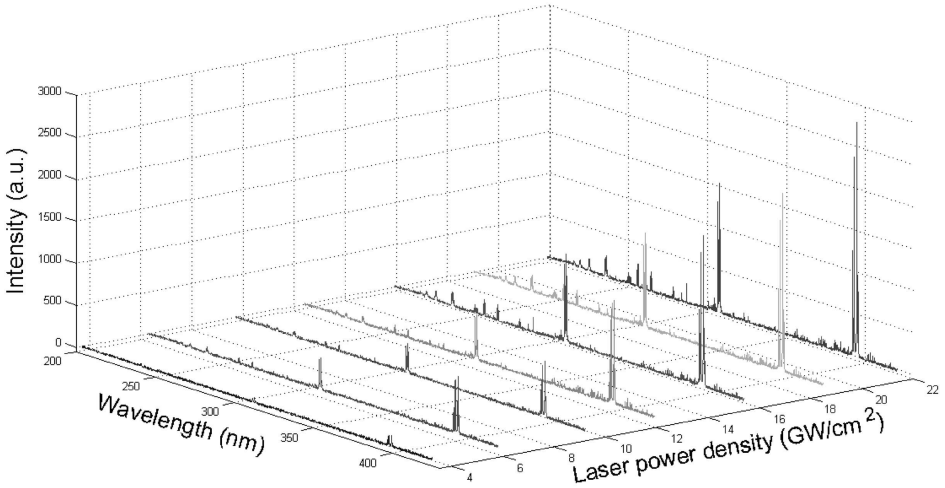

Figure 5. Emission spectra of the laser-induced aluminum alloy plasma with different laser power densities at a distance of 0.5 mm above the target surface.

the intensities of the spectra increase with the increase in the laser power density. With the increase in the laser irradiance, the mass ablation rate also increases which results in the increase of the spectral line intensities [28]. At the same time, in figure 6, we can see that the emission curves, which show a rapid linear increase at low power densities, start to bend when 6.3 GW/cm^2 is reached with a flat region. For laser power densities above 9.7 GW/cm^2, a new increase of the emission intensities is produced. Aguilera *et al* observed similar phenomenon in their experiments [29]. They put forward two models to explain this phenomenon. For the lower power

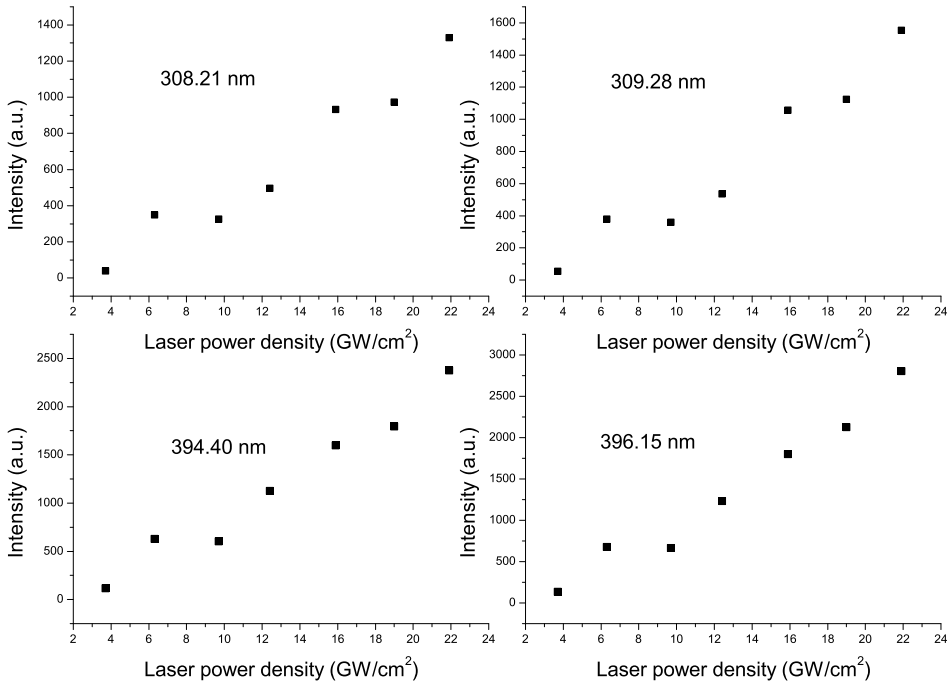

Figure 6. Variation of the intensities of four emission lines (308.21, 309.28, 394.40 and 396.15 nm) with different laser power densities at 0.5 mm above the target surface.

densities, a laser-supported detonation wave is expected and more power will be absorbed and produce an increase in plasma height and plasma emission. At the region of higher power densities, above 9.7 GW/cm^2 in our case, this new increase of the atomic emission could be explained by the change of the absorption mechanism to a laser-supported radiation wave at which the plasma temperature is so high that the shielding effect of the plasma decreases and at the same time the plasma becomes relatively transparent to the laser beam and the ablation of the target is again enhanced [29,30]. So the emission of the high-temperature plasma is in agreement with our results.

The variations of excitation temperature and electron number density with laser power density at a distance of 0.5 mm from the target surface were also studied. As the laser power density increases from 3.7 to 21.9 GW/cm^2, N_e increases from 2.45×10^{17} to 3.15×10^{17} cm^{-3}, and T_e varies from 6085 to 7498 K. At the lower irradiance levels, the mass ablation rate increases rapidly with the increase in the laser irradiance. Hence, N_e and T_e increase obviously. However, at higher irradiance, the saturation of N_e and T_e occurs. This is because the increase in the electron number density and temperature with the increase in the laser power density is due to the absorption and/or reflection of the laser photon by the plasma [31]. The plasma frequency is given as $\nu_p = 8.9 \times 10^3 N_e^{1/2}$ [32]. As the electron density increases, the plasma frequency also will increase. As soon as ν_p becomes

larger than the laser frequency, the laser radiation will be reflected. For a 1064 nm Nd:YAG laser, the corresponding frequency $\nu_l = 2.82 \times 10^{14}$ Hz which is much larger than the plasma frequency $\nu_p \approx 5.0 \times 10^{12}$ Hz considering the maximum electron number density (3.1×10^{17} cm^{-3}). Therefore, the loss of energy due to reflection of the laser beam from the plasma can be assumed to be insignificant.

Other reasons for the saturation of N_e and T_e at higher irradiance levels are the absorption mechanisms of the laser-induced plasma. In our work, two dominant mechanisms are responsible for plasma absorption at high laser power densities. One is photoionization (PI) of the excited or the ground state atoms. As the photon energy of the 1064 nm laser (1.17 eV) is much lower than the excitation potentials of atomic transitions of aluminum and silicon atoms (5.98 and 8.15 eV, respectively) [24], the direct photoionization by the absorption of a laser photon is ruled out. The only possibility for photoionization absorption to occur is by simultaneous absorption of a number of photons, which is obviously less efficient for the 1064 nm laser.

The second absorption mechanism is the inverse bremsstrahlung (IB) absorption. In the IB process, the free electrons gain kinetic energy from the laser beam, and the IB absorption via free electrons is approximated as [26]

$$\alpha_{IB}(\text{cm}^{-1}) = 1.37 \times 10^{-35} \lambda^3 N_e^2 T_e^{1/2}, \tag{5}$$

where λ (μm) is the wavelength of the laser photons, T_e (K) is the electron temperature and N_e (cm^{-3}) is the electron number density. The above equation clearly illustrates that the IB process is very efficient for the IR laser considering its λ^3 dependence. At the same time, we note that the absorption through inverse bremsstrahlung is very small at lower laser power densities and increases exponentially with the increase of laser irradiance leading to the saturation of N_e and T_e at higher laser power densities. Harilal *et al* [26] observed similar variations of N_e and T_e with the increasing laser irradiance and pointed out that the saturation in N_e and T_e at higher irradiance levels cannot be explained by considering only the prominent absorption mechanisms via IB and PI. They put forward a self-regulating model at higher irradiance to explain such temperature and density variations. This assumption was found to be valid in laser-generated plasma where thermalization time is significantly less than the plasma expansion time, resulting in uniform temperature in the local region of the plasma.

3.5 *Spatial evolution of the plasma spectra, T_e and N_e*

In order to study the spatial evolution of the plasma spectra, the electron temperature and the electron number density, the laser power density is adjusted to 6.3 GW/cm^2. The spectra were recorded at different axial heights above the target surface, from 0.1 to 4.0 mm, and no signal can be discriminated from the noise above 4.0 mm.

Figure 7 shows the spatial distribution of the integral intensities of four neutral aluminum lines (308.21, 309.28, 394.40, 396.15 nm). As can be seen, intensities of the signals increase rapidly near the target surface, and reach the maximum at a distance of about 1.5 mm from the target surface, then decrease with the increase in

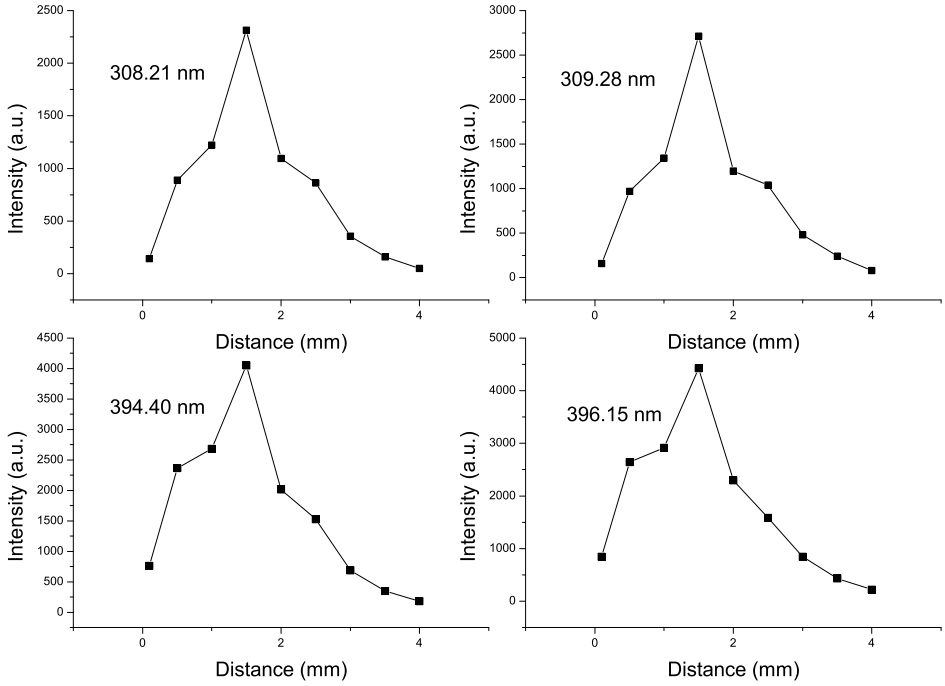

Figure 7. Variation of the spectra along the direction of propagation of the plume at a laser power density of 6.3 GW/cm^2.

distance. The line emission intensities reflect the temperature distribution within the plume which will be discussed below.

The variation of the electron temperature along the direction of propagation of the plume is presented in figure 8. A slight decrease of temperature at both the plasma edge and close to the target surface was observed. The drop in the temperature near the surface of the target results from the thermal conduction from the plasma towards the aluminum alloy considering the equipartition time for energy transfer from electrons to ions (10^{-10}–10^{-11} s) [33]. In nanosecond laser heating of metals, the target is heated up to the melting point and then to the vapourization temperature by the absorption of laser energy. In this case, the main sources of energy loss are the evaporation from the liquid metal and the heat conduction into the solid target. The high value of the electron temperature observed in the range of 1.5−2.5 mm from the target surface is due to absorption of the laser energy by means of electrons via IB absorption process, and is consistent with the spatial variation of the line emission intensity. Margetic *et al* [34] used the laser-sustained detonation model to explain similar phenomenon. A strong compression of the front of the plume at the initial stage of the plasma evolution creates an absorbing zone for the laser light, which results in a rise in temperature at the back side of the plume front. In 2003, Hafez *et al* studied the temperature spatial distribution of laser-induced Cu plasma using a 335 nm pulsed Nd:YAG laser. They found that the maximum attainable value of electron temperature was

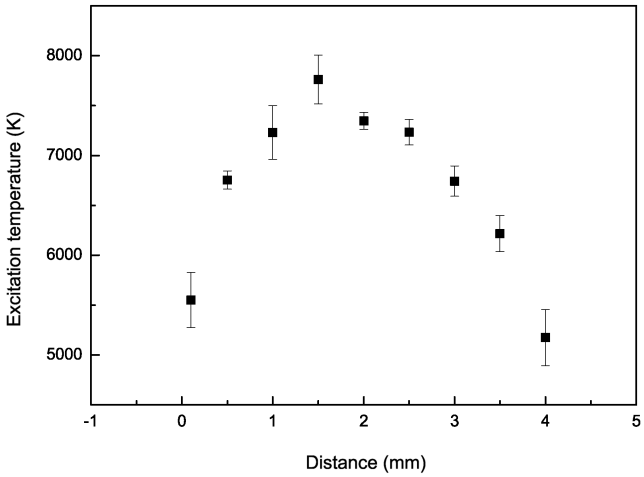

Figure 8. Variation of the excitation temperature along the direction of propagation of the plume at a laser power density of 6.3 GW/cm^2.

at a distance of 2–3 mm away from the target surface [35]. This behaviour is also in agreement with ours. At the same time, the decrease of temperature near the target surface can be understood in another way. The ionization potentials of Si, Fe, Cu, Mn, Mg, Ni, Zn, Ti and Ga are 8.15, 7.90, 7.72, 7.43, 7.65, 7.64, 9.39, 6.82 and 6.00 eV, while that of Al is 5.98 eV [24]. To increase the trace elements means to increase portion of the laser–target interaction volume of the trace elements and decrease the laser–target interaction volume of the major element aluminum. Therefore, the value of T_e near the target surface will decrease with the increase in the trace elements in the aluminum alloy sample [36].

As for the decrease in electron temperature at the plasma edge, two reasons should be considered. One is the radiative cooling which is higher in this area because of the larger emitting surface. The other is that the thermal energy is rapidly converted into kinetic energy causing the temperature to drop off rapidly as the plasma expands. The spatial dependence of the electron temperature has been studied by many other researchers also [18,26,31]. Their studies showed that the temperature was decreased with distance. The difference between ours and theirs further indicates that the laser–matter interaction is so complicated that further study of laser-induced plasma parameters is needed.

The electron density at a distance of 0.1 mm above the target surface is approximately 2.9×10^{17} cm^{-3} and decreases to about 1.9×10^{17} cm^{-3} at a distance of 4 mm. The high electron density near the target is due to the high absorption of the incident laser beam energy in the earlier formed plasma. As the plasma expands, recombination between electron and ion becomes predominant. On the trailing edge of the laser pulse, the electron recombination cannot be compensated by the production of free electrons because of the decrease of the laser irradiance. This is consistent with previous conclusions [26,31].

3.6 *LTE and self-absorption analysis*

To determine the electron temperature, the plasma must satisfy the equilibrium conditions, i.e. the plasma must hold a state of local thermodynamic equilibrium during the observation window. In an LTE plasma, the collisional excitation and de-excitation processes must dominate radiative processes and this requires a minimum electron density. The lower limit of the electron density for which the plasma will be in LTE is [37]

$$N_{\mathrm{e}}\ (\mathrm{cm}^{-3}) \geq 1.4 \times 10^{14} T^{1/2}\ (\mathrm{eV})[\Delta E\ (\mathrm{eV})]^3, \tag{6}$$

where ΔE (eV) is the difference between the upper and lower states and T (eV) is the temperature. For the Si(I) 288.16 nm line transition, $\Delta E = 4.3$ eV, and the highest electron temperature observed was approximately 7762 K. From eq. (6), a minimum electron density of 9.1×10^{15} cm^{-3} is required for LTE to hold, which is much lower than the N_{e} (10^{17} cm^{-3}) obtained in our experiments. Therefore, local thermodynamic equilibrium is valid for the condition of the present plasma.

On the other hand, when evaluating the electron temperature using Boltzmann plot method and the electron number density using spectral line broadening, it is important to verify that the plasma is not optically thick for the lines used. If the plasma is optically thin, the intensities should be in a ratio that is consistent with the ratio of their statistical weights, and we found it to be the case in our experiments. Take the transitions 3d $^2D_{3/2} \rightarrow$ 3p $^2P_{1/2}$ (308.21 nm) and 3d $^2D_{3/2} \rightarrow$ 3p $^2P_{3/2}$ (309.28 nm) for example. The experimentally obtained transition probability ratios are 0.71961 at 3.7 GW/cm^2, 0.92058 at 6.3 GW/cm^2, 0.90811 at 9.7 GW/cm^2, 0.92619 at 12.4 GW/cm^2, 0.88295 at 15.9 GW/cm^2, 0.86479 at 19.0 GW/cm^2 and 0.85521 at 21.9 GW/cm^2, respectively. The average value 0.868206 is in excellent agreement with the data 0.85135 in the NIST database considering the experimental uncertainty. This further indicates that the plasma tested was optically thin.

4. Conclusions

In this paper, a transient and elongated plasma was produced by focussing the radiation from a 1064 nm Q-switched Nd:YAG onto the aluminum alloy in air at atmospheric pressure. The plasma parameters (electron number density and electron temperature) were studied using spectroscopic technique at several locations in front of the target surface and with seven different laser power densities. The electron density inferred by measuring the Stark-broadened line profile of Si(I) 288.16 nm becomes maximum near the target surface and decreases with increasing distance from the target surface for recombination with ions. The electron temperature was determined using the Boltzmann plot method with nine neutral aluminum lines (236.69, 256.80, 257.51, 265.24, 266.04, 308.215, 309.284, 394.401 and 396.152 nm). Due to the thermal conduction towards the solid target and radiative cooling of the plasma as well as conversion of thermal energy into kinetic energy, the electron temperature decreases both at the plasma edge and close to the target surface.

With an increase in laser irradiance, both electron density and electron temperature increase at lower irradiance levels and saturate at higher irradiance levels. The saturation of electron density and temperature at these irradiance levels is expected to be due to the inverse bremsstrahlung process considering the energy of the 1064 nm laser photon only to be 1.17×10^{-3} eV. Two models (laser-supported detonation wave and laser-supported radiation wave) were used to explain the characteristics of the plasma spectra at different laser power densities.

According to the experimental results, the assumption of local thermodynamic equilibrium was valid. The experimentally obtained transition probability ratios at seven laser irradiance were studied and the results were in excellent agreement with the NIST database. This demonstrated that the plasma tested was optically thin.

Acknowledgements

This research was supported by the CAS/SAFEA International Partnership Program for Creative Research Teams.

References

[1] J M Gomba, C D'Angelo, D Bertuccelli and G Bertuccelli, *Spectrochim. Acta Part B* **56**, 695 (2001)
[2] D A Cremers and L J Radziemski, *Handbook of laser-induced breakdown spectroscopy* (John Wiley & Sons, Ltd, Chichester, 2006)
[3] A W Miziolek, V Palleschi and I Schechter, *Laser-induced breakdown spectroscopy (LIBS): Fundamentals and applications* (Cambridge University Press, New York, 2006)
[4] J S Cowpe, R D Pilkington, J S Astin and A E Ahill, *J. Phys. D: Appl. Phys.* **42**, 165202 (2009)
[5] S Amoruso, R Bruzzese, N Spinelli and R Velotta, *J. Phys. D: Appl. Phys.* **32**, R131 (1999)
[6] R E Russo, X L Mao, H Liu, J Gonzalez and S S Mao, *Talanta* **57**, 425 (2002)
[7] S Pandhija and A K Rai, *Pramana – J. Phys.* **70**, 553 (2008)
[8] K Y Yamamoto, D A Cremers, M J Ferris and L E Foster, *Appl. Spectrosc.* **50**, 222 (1996)
[9] R Noll, H Bette, A Brysch, M Kraushaar, I Moench, L Peter and V Sturm, *Spectrochim. Acta Part B* **56**, 637 (2001)
[10] A Uhl, K Loebe and L Kreuchwig, *Spectrochim. Acta Part B* **56**, 795 (2001)
[11] L Burgio, K Melessanaki, M Doulgeridis, R J H Clark and D Anglos, *Spectrochim. Acta Part B* **56**, 905 (2001)
[12] S R Goode, S L Morgan, R Hoskins and A Oxsher, *J. Anal. At. Spectrom.* **15**, 1133 (2000)
[13] A K Knight, N L Scherbarth, D A Cremers and M J Ferris, *Appl. Spectrosc.* **54**, 331 (2000)
[14] M Autin, A Briand and P Mauchien, *Spectrochim. Acta Part B* **48**, 851 (1993)
[15] J B Simeonsson and A W Miziolek, *Appl. Phys.* **B59**, 1 (1994)
[16] J M Anzano, I B Gornushkin, B W Smith and J D Winefordner, *Polym. Eng. Sci.* **40**, 2423 (2000)

[17] L C Jensen, S C Langford, J T Dickinson and P S Addleman, *Spectrochim. Acta Part B* **50**, 1501 (1995)
[18] N M Shaikh, S Hafeez, B Rashid, S Mahmood and M A Baig, *J. Phys. D: Appl. Phys.* **39**, 4377 (2006)
[19] N M Shaikh, B Rashid, S Hafeez, S Mahmood, M Saleem and M A Baig, *J. Appl. Phys.* **100**, 073102 (2006)
[20] N M Shaikh, B Rashid, S Hafeez, Y Jamil and M A Baig, *J. Phys. D: Appl. Phys.* **39**, 1384 (2006)
[21] N M Shaikh, S Hafeez, B Rashid and M A Baig, *Eur. Phys. J.* **D44**, 371 (2007)
[22] A Elhassan, A Giakoumaki, D Anglos, G M Ingo, L Robbiola and M A Harith, *Spectrochim. Acta Part B* **63**, 504 (2008)
[23] G Cristoforetti, S Legnaioli, V Palleschi, A Salvetti and E Tognoni, *Spectrochim. Acta Part B* **59**, 1907 (2004)
[24] http://physics.nist.gov/PhysRefData/ASD/index.html
[25] J S Cowpe, J S Astin, R D Pilkington and A E Hill, *Spectrochim. Acta Part B* **63**, 1066 (2008)
[26] S S Harilal, C V Bindhu, R C Issac, V P N Nampoori and C P G Vallabhan, *J. Appl. Phys.* **82**, 2140 (1997)
[27] V Narayanan and R K Thareja, *Appl. Surf. Sci.* **222**, 382 (2004)
[28] R E Russo, X L Mao, H C Liu, J H Yoo and S S Mao, *Appl. Phys.* **A69**, S887 (1999)
[29] J A Aguilera, C Aragon and F Penalba, *Appl. Surf. Sci.* **127**, 309 (1998)
[30] M Von Allmen and A Blatter, *Laser-beam interaction with materials – Physical principles and applications*, 2nd ed. (Springer-Verlag, Berlin, 1995)
[31] S Hafeez, N M Shaikh and M A Baig, *Laser and Particle Beams* **26**, 41 (2008)
[32] R K Singh, O W Holland and J Narayan, *J. Appl. Phys.* **68**, 233 (1990)
[33] S Amoruso, M Armenante, V Berardi, R Bruzzese and N Spinelli, *Appl. Phys.* **A65**, 265 (1997)
[34] V Margetic, A Pakulev, A Stockhaus, M Bolshov, K Niemax and R Hergenroder, *Spectrochim. Acta Part B* **55**, 1771 (2000)
[35] M A Hafez, M A Khedr, F F Elaksher and Y E Gamal, *Plasma Sources Sci. Technol.* **12**, 185 (2003)
[36] Walid Tawfik and Y Mohamed, *Prog. Phys.* **2**, 87 (2007)
[37] G Abdellatif and H Imam, *Spectrochim. Acta Part B* **57**, 1155 (2002)